Journal of proteome research

Article

pubs.acs.org/jpr

Early Events in Plastid Protein Degradation in *stay-green Arabidopsis* Reveal Differential Regulation beyond the Retention of LHCII and Chlorophyll

Julia Grassl,[†,‡] Adriana Pružinská,[†,‡] Stefan Hörtensteiner,[§] Nicolas L. Taylor,[†,‡] and A. Harvey Millar*[,†,‡]

[†]ARC Centre of Excellence in Plant Energy Biology and [‡]Centre for Comparative Analysis of Biomolecular Networks (CABiN), Bayliss Building M316, The University of Western Australia, 35 Stirling Highway, Crawley WA 6009, Western Australia, Australia

[§]Zurich-Basel Plant Science Center, Institute of Plant Biology, University of Zurich, CH-8008 Zurich, Switzerland

Supporting Information

ABSTRACT: An individually darkened leaf model was used to study protein changes in the *Arabidopsis* mutant *stay-green1* (*sgr1*) to partially mimic the process of leaf covering senescence that occurs naturally in the shaded rosettes of *Arabidopsis* plants. Utilizing this controlled and predictable induced senescence model has allowed the direct comparison of *sgr1* with Col-0 during the developmental period preceding the retention of chlorophyll and light harvesting complex II (LHCII) in *sgr1* and the induction of senescence in Col-0. Quantitative proteomic analysis of soluble leaf proteins from *sgr1* and Col-0 before the initiation of senescence has revealed a range of differences in plastid soluble protein abundance in *sgr1* when compared to Col-0. Changes were also observed in membrane located machinery for photosystem II (PSII), in Calvin cycle components, proteins involved in redox control of the stromal compartment and ammonia assimilation that differentiated *sgr1* during the early stages of the senescence process. The changes in PSII abundance were accompanied with a lower capacity of photosynthetic CO_2 assimilation in *sgr1* than Col-0 after return of plants to lighted conditions following 3 and 5 days of darkness. A light-harvesting chlorophyll-a/b binding protein (LHCB2) was retained during the later stages of senescence in *sgr1* but this was accompanied by an enhanced loss of oxygen evolving complex (OEC) subunits from PSII, which was confirmed by Western blotting, and an enhanced stability of PSII repair proteins in *sgr1*, compared to Col-0. Together these data provide insights into the significant differences in the steady-state proteome in *sgr1* and its response to senescence, showing this cosmetic stay-green mutant is in fact significantly different to wild-type plants both before and during leaf senescence.

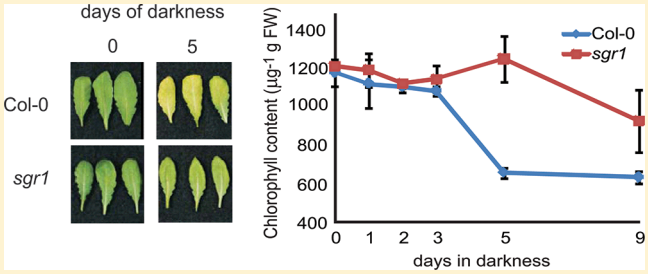

KEYWORDS: *sgr, LHC, leaf senescence*

INTRODUCTION

The loss of chlorophyll (Chl) and yellowing of leaves is a prominent characteristic of plant senescence.[1] Mutants that retain green pigments during senescence are collectively called "stay-green" mutants and have been identified as belonging to either functional or cosmetic stay-green phenotypes. In the functional group, the mutants have altered developmental patterns and timing of senescence.[2,3] The cosmetic phenotypes (also called type C stay-green) are associated with alteration in the timing and extent of Chl breakdown, but in the background, the leaf senescence program appears to be progressing normally.[4] These mutants have become a useful tool to study the Chl breakdown process and its consequences and most are thought to represent mutants that have a defect in a catalytic or regulatory gene of Chl breakdown.[1] In *Arabidopsis*, three type C stay-green genes have been identified: PaO, NYC1 (chlorophyll *b* reductase) and SGR.[4] In 2007, research by several independent groups led to the identification of SGR from different plant species, that is, *Festuca prantensis*,[5] *Arabidopsis*,[6] rice,[7] and pea.[8] The latter was of particular interest from a historical point of view as the gene responsible for the green cotyledon phenotype in pea was one of the seven traits Gregor Mendel used to determine the laws of Mendelian inheritance in garden peas.[5,8]

SGR is a senescence-associated gene that is typically upregulated during senescence; *nye1* mutants in *Arabidopsis* show a nonyellowing phenotype during natural and dark-induced senescence.[6] The proteins encoded by SGR genes from different species are 25−30 kDa and lack a clear transmembrane domain or any other known protein domains other than the one defined by the SGR family (PF12638). Homologues of SGR are found among higher plants, moss and algae, and are related to bacterial proteins of unknown function in anaerobic bacteria, notably of the genus *Clostridium*. In rice and *Arabidopsis*, SGR is located in the plastids of cells suggesting a direct role in the initiation of a plastid-localized degradation event that regulates chlorophyll degradation.[6,7]

Received: July 26, 2012
Published: October 2, 2012

dx.doi.org/10.1021/pr300691k | *J. Proteome Res.* 2012, 11, 5443−5452

Transient overexpression of *SGR* and *in vivo* pull-down assays have shown that SGR interacts directly with LHCPII in rice and that SGR-LHCPII complexes are formed in thylakoid membranes.[7] However, a missense mutation in rice SGR (V99M) does not affect the binding activity to LHCPII, showing that the functional impairment of this mutation is not associated with photosystem II (PSII) binding per se.[7] In addition to the retention of chlorophyll, the LHCs of PSII appear to remain intact and stacked during senescence in the mutant, while the complex is disassembled in wild-type (WT) plants. Recently, five chlorophyll catabolism enzymes (CCEs) were shown to specifically interact with LHCII and SGR was essential for recruiting CCEs in senescing chloroplasts. The SGR-CCE-LHCII interaction during the breakdown of LHCII-located chlorophyll was proposed to allow the metabolic channelling of phototoxic Chl breakdown intermediates.[9]

Despite these recent advances, there is still little information on the broader biochemical processes in plastids that differ in *sgr* mutants during the early stages of senescence. To frame the events that lead to, or correlate with, the later differential stability of the LHCII core subunits and the retention of Chl in *sgr* mutants, more information at the protein level is needed. While LHCs stay intact during dark-induced senescence in *sgr* mutants, the efficiency of PSII and the rate of photosynthesis have been shown to decline in the same manner as WT.[6] Hence, it seems likely that some factor or factors related to PSII function are changing in *sgr* considering the role of PSII in photosynthesis and Chl fluorescence. Also, while senescence is not visually apparent in *sgr*, it seems plausible that other protein components will be altered in this mutant. These changes are likely the cause of alterations in fresh weight and pathogenic responses of the mutant when compared to matched WT plants.[2,10−12] Here we report, using quantitative proteomics, changes in PSII, in Calvin cycle components, in proteins involved in redox control of the stromal compartment and in ammonia assimilation that differentiated *Arabidopsis sgr1* during the early stages of the senescence process. The light-harvesting chlorophyll-a/b binding protein (LHCB2) was retained during the later stages of senescence in *sgr1* but this was accompanied by an enhanced loss of oxygen evolving complex (OEC) subunits, explaining the loss of photosynthetic capacity of *sgr1* during senescence.

■ MATERIALS AND METHODS

Plant Growth Conditions and Measurements

Arabidopsis thaliana (ecotype Columbia-0) and RNAi line *sgr1 #2* (termed *sgr1*;[5,13]) were grown in soil under short-day (8 h day/16 h night) conditions with fluorescent light of 150 μmol photons m^{-2} s^{-1} at 22 °C and 65% relative humidity. For induction of senescence, leaves from 8-week-old plants were individually covered with aluminum foil for up to 9 days.

Chl abundance was quantified at various time points from leaves of control and covered leaves at 0−9 days of darkness. Leaves were frozen in liquid nitrogen and stored at −80 °C. Chl was extracted with 80% (v/v) acetone. Chl absorbance was measured spectrophotemetrically at 647 and 663 nm and the total Chl content determined as $[7.15 \times (A_{663} - A_{750}) + 18.71 \times (A_{647} - A_{750})]$.

Chl fluorescence and the photochemical efficiency of PSII (measured as F_v/F_m) was also quantified at various time points from leaves of control and covered leaves at 0−9 days of darkness using a IMAGING−PAM (Walz) according to the manufacturer's instructions.

Semiquantitative RT-PCR

RNA extraction, DNase treatment, and first-strand cDNA synthesis were performed according to the manufacturer's instructions using the Qiagen RNeasy kit and SuperScript III reverse transcriptase (Invitrogen). PCR was performed for 30−35 cycles with gene-specific primers as follows for SGR1 (AT4G22920): SGR1-L, ACAAGTTCCCATCTCCATGC; and SGR1-R, GGAAAATGTCGCTTCACGTT. For SAG12 (AT5G45890): SAG12-L, TCCTTACAAAGGCGAAGACG; and SAG12-R, TCATTAACCGGGACATCCTC. For WRKY53 (AT4G23810): WRKY53-L, CAGACGGGGATGCTACGG; and WRKY53-R, GGCGAGGCTAATGGTGGTG, with actin as a control. For actin2-8 (AT3G18780-AT1G49240): Actin L, GGTAACATTGTGCTCAGTGGTGG; and Actin R, AACGACCTTAATCTTCATGCTGC. For PAO (At3g44880): PAO-L GTTTCCAAGGTGCGAATGAT; PAO-R ACCGACGATTGGTAGTTTCG, (size 108 bp). PCR products were visualized on an agarose gel stained with ethidium bromide. Fragment sizes for SGR1 (141 bp), SAG12 (93 bp), WRKY53 (91 bp), and actin (107 bp) were all of the expected size.

Protein Extraction and Quantification

All protein extraction and purification steps were carried out keeping samples on ice or at 4 °C. Leaves were collected and immediately frozen in liquid N_2. Total protein extracts were prepared by grinding the tissue using a pestle and mortar and solubilization with extraction buffer (50 mM Tris-HCl, 10% (v/v) glycerol, 0.05% (v/v) β-mercaptoethanol and complete, mini protease inhibitor cocktail (Roche) pH 7.5). The homogenate was vortexed shortly and clarified by filtering through miracloth (Merck Millipore). The filtrate was then centrifuged at 300*g* for 2 min at 4 °C to remove all plant cell debris. The supernatant was collected and centrifuged at 20 000*g* for 20 min to separate soluble and membrane proteins. The soluble fraction was collected and the concentration of total protein was determined using a Bradford assay (Pierce).

Western Blotting

Soluble protein extracts (2 μg protein or 0.75 mg of FW) and membrane proteins (3.3 μg protein or 3.3 mg of FW) were separated by SDS-PAGE on 10−20% Criterion Tris-HCl polyacrylamide gels (BioRad). For immunodetection, separated proteins were then transferred to Hybond-C Extra nitrocellulose membranes (GE Healthcare Life Sciences) using a semidry apparatus (Hoefer) and incubated at room temperature for 1 h with primary antibodies. Primary antibodies to PSII subunits were all purchased from Agrisera. Appropriate secondary antibodies conjugated to horseradish peroxidase were applied to washed membranes for 1 h prior to allow detection of the chemiluminescent signal using the ECL Advance Western Blotting Detection Kit (GE Healthcare Life Sciences) and an ImageQuant RT ECL imager (GE Healthcare Life Sciences) by standard procedures.

Protein Labeling and Fractionation

For each sample, 100 μg of protein was precipitated by the addition of 4 vol of cold acetone and stored in −20 °C overnight. The precipitated protein was then centrifuged at 20 000*g* for 20 min and the resulting pellet was then resuspended in dissolution buffer, denatured, and cysteines were blocked according to the manufacturer's instructions (iTRAQ Reagents

-8plex Amine-modifying Labeling Reagents for Multiplexed Relative and Absolute Protein Quantitation, Revision C, AB Sciex). Each sample was digested by addition of 10 μL of 1 μg/μL trypsin (Invitrogen) at 37 °C overnight and labeled with the iTRAQ reagents (according to the manufacturer's instructions) in triplicate in the following experiments: (i) 0dd Col-0, 114, 117, and 119; 0dd *sgr 1*, 115, 116, and 121. (ii) 3dd Col-0, 115, 117, and 119; 3dd *sgr 1*, 114, 118, and 121. (iii) 5dd Col-0, 113, 116, and 121; 5dd *sgr 1*, 114, 115, and 119. The labeled samples were pooled prior to further analysis. To remove excess labeling reactants and to reduce interference of salts during LC−MS/MS analysis, the pooled samples were divided in two aliquots. One aliquot was diluted 4-fold with SCX buffer A (10 mM KH_2PO_4 in 25% (v/v) acetonitrile (ACN), pH 3.0) and subjected to strong cation exchange (SCX) chromatography using an OPTI-LYNX cartridge (Optimize Technologies). The eluent was dried in a vacuum concentrator and stored at −20 °C for LC−MS/MS analysis. The other aliquot (300 μg) was separated into 1 min fractions over a 35 min gradient 0−60% buffer B (10 mM $KHPO_4$ in 1 M KCl and 25% [v/v] ACN, pH 3) SCX column (4.6 mm, 10 cm, 300 A, PolyLC, Columbia, MD). The fractions were dried *in vacuo* and desalted using C18 cartridges (Nest Group).

Mass Spectrometry

Samples were analyzed on an Agilent 6510 Q-TOF mass spectrometer with an HPLC Chip Cube source. The chip consisted of a 160 nL enrichment column (Zorbax 300SB-C18 5 μm) and a 150 mm separation column (Zorbax 300SB-C18 5 μm) driven by Agilent Technologies 1100 series nano/capillary liquid chromatography system. Both systems were controlled by MassHunter Workstation Data Acquisition for Q-TOF (ver B.2.00, Agilent Technologies). Peptides were loaded onto the trapping column at 4 μL min^{-1} in 5% (v/v) ACN and 0.1 (v/v) % formic acid with the chip switched to enrichment and using the capillary pump. The chip was then switched to separation and peptides eluted during a 1 h gradient (5%−40% ACN) directly into the mass spectrometer. The mass spectrometer was run in positive ion mode and MS scans run over a range of m/z 275−1500 and at a scan rate of 4 spectra s^{-1}. Precursor ions were selected for auto MS/MS at an absolute threshold of 500 and a relative threshold of 0.01, with max 3 precursors per cycle, and active exclusion set at 2 spectra and released after 1 min. Precursor charge-state selection and preference was set to 2+ and 3+ and precursors selected by charge then abundance. Resulting MS/MS spectra were opened in MassHunter Workstation Qualitative Analysis (ver B.03.01, Agilent Technologies) and MS/MS compounds detected by "Find Auto MS/MS" using default settings. The resulting compounds were then exported as .mzdata files. Multiple SCX fractions and exclusions runs were combined using mzdataCombinator v1.0.4 (The West Australian Centre of Excellence in Computational Systems Biology, http://www.plantenergy.uwa.edu.au/wacecsb/software.shtml) and resulting files were searched against the TAIR 10 database for *A. thaliana* protein sequences (33 621 protein sequences, 13 487 170 residues) using Mascot ver 2.3 (Matrix Science). The following settings were selected for database searching: MS error tolerance of ±100 ppm, MS/MS error tolerance of ±0.5 Da, maximum missed cleavages tolerated as 1; fixed modifications methylthio (C), iTRAQ8plex (N-term), iTRAQ8plex (K) and variable modifications oxidation (M) and iTRAQ8plex (Q), peptide charge as 2^+ and 3^+ and finally, the instrument selected as ESI-Q-ToF. For initial analysis protein score, >46 was used as a threshold for identification and subsequent quantification. For proteins in this set classified as plastid, based on experimental published evidence as outlined in Supplementary Data S1, a further Mascot ion score cut off (34 or 35), was used to yield a false discovery rate of <5% at the peptide level for identifications, when searching with the Mascot Decoy function enabled. Quantitation of all spectra for each protein was carried out using default settings in Mascot ver 2.3 (Matrix Science) for quantitation on isobaric mass tags (iTRAQ) at the peptide level. For proteins reported to have a non-normal distribution, the geometric standard deviation was determined manually. Here a geometric mean for the individual peptide ratios and a 95% CI window was calculated as a *t*-test in Analyze-it v.2.21 (Microsoft Excel) to provide statistical confidence in the changes in abundance reported between *sgr1* and Col-0. Details of fold changes, quality of matches and number of peptides with ion scores above 34/35 for each identification are provided in Supplementary Data S1. Proteins without peptides above the ion cut off were excluded, proteins with single peptides hits were manually inspected, and the MS/MS spectrum is shown in the Supplementary Data 2.

Measurement of Photosynthetic Rate and Gas Exchange

Gas-exchange parameters, including photosynthetic rate, CO_2 assimilation rate, transpiration, and stomatal conductance, were measured on control and covered leaves from both WT and *sgr1* plants using a LI-6400 XT infrared gas analyzer (Li-Cor). All measurements were carried out after at least 2 h of illumination. Per plant, five leaves were enclosed in a 6-cm^2 leaf chamber. Data was collected after acclimation of the leaf to conditions similar to their growth conditions (light intensity of 300 μmol m^{-2} s^{-1}, relative humidity of 60−70%, temperature of 22 °C, and 400 ppm CO_2).

RESULTS

Defining the Timing of Senescence Induced Chl Degradation in Col-0 and *sgr1*

To determine if the *sgr1* mutant exhibits a stable stay-green phenotype during dark-induced senescence, leaves still attached to the mutant and WT type plants were placed in darkness for up to 9 days by leaf covering with aluminum foil. The leaves of the mutant remained green on the third day after darkness (3dd) and turned to light green after 5dd. In contrast, WT leaves became light green on 3dd and turned yellow after 5dd (Figure 1A).

The chlorophyll (Chl) content of darkened leaves was determined by Chl extraction in acetone and spectrophotometry. Much of the Chl content was retained in the mutant after dark treatment, whereas it was degraded rapidly between 3dd and 5dd in WT plants (Figure 1B). In contrast, the maximal photochemical efficiency (F_v/F_m) of PSII degraded in a similar manner in the WT and *sgr1* following exposure to darkness. While F_v/F_m was slightly higher in the WT at 7dd than in *sgr1*, the difference was not significant (Figure 1C). This indicated that the senescence-related decline of photosynthetic electron transport was not affected by the *sgr1* mutation (Figure 1C), consistent with its designation as a C-type stay-green mutant. The *sgr1* line is one of a number of lines generated that express an RNAi construct for *SGR1*, reducing the steady-state transcripts level of *SGR1*.[5] To confirm reduction of *SGR1* expression, RT-PCR analysis was performed during leaf senescence experiments. A significantly reduced amount of

dx.doi.org/10.1021/pr300691k | J. Proteome Res. 2012, 11, 5443−5452

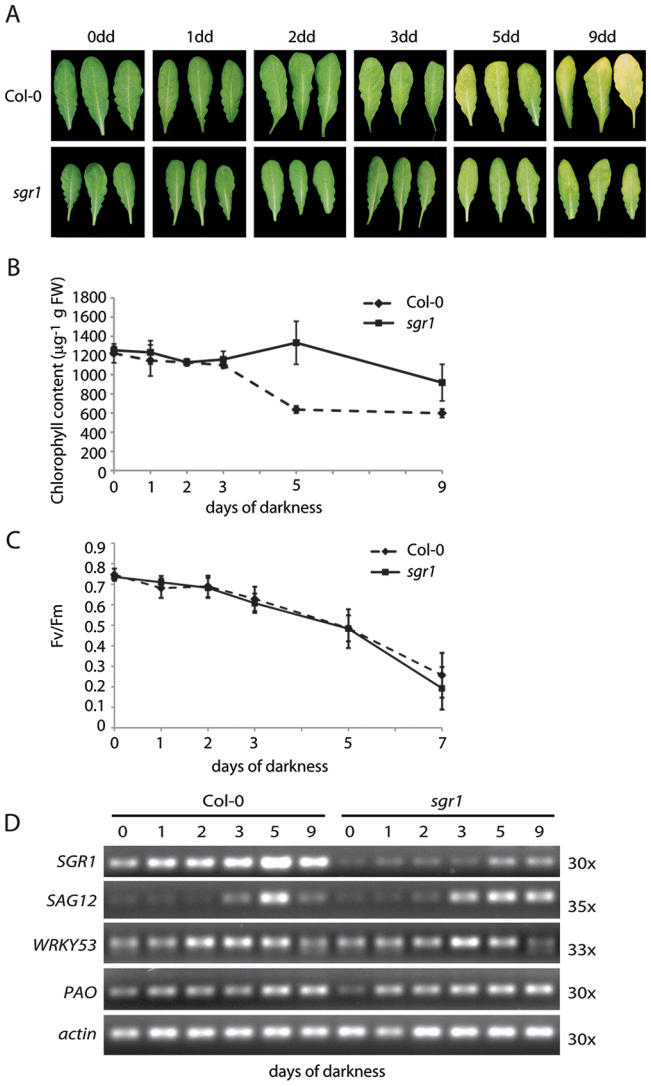

Figure 1. Phenotypic characterization of *sgr1*. (A) Representative Col-0 and *sgr1* leaves during dark-induced senescence over 9 d. (B) Total chlorophyll content in Col-0 and *sgr1* during dark-induced senescence. Error bars represent standard deviation (n = 4). (C) Photochemical efficiency of PSII in Col-0 and *sgr1* during dark-induced senescence. F_v/F_m, maximum quantum yield for PSII electron transport. Error bars represent standard deviation (n = 4). (D) RT-PCR analysis of *SGR1*, *SAG12*, *WRKY53*, *PAO*, and *actin* during dark-induced senescence. The number of cycles is shown to the right.

SGR1 transcript was observed in the mutant at all time points during dark-induced senescence (Figure 1D). The senescence-associated gene *SAG12*, the transcription factor *WRKY53* and *PAO* (pheophorbide *a* oxygenase), all previously shown to be senescence-induced, showed similar transcript accumulation as senescence progressed in both *sgr1* and WT. Together, these results show an altered Chl stability during dark-induced senescence in *sgr1*, but no difference in the efficiency of PSII or in the induction of senescence-associated genes.

The Dynamics of Protein Degradation and LHC Retention during Senescence

An understanding of the rate and degree of protein degradation during senescence is a necessary prerequisite to the study and interpretation of proteome variations between *sgr1* and WT plants. Assessment of total protein abundances by examining SDS-PAGE gels and soluble proteins by colormetric assays both showed that between 0dd and 3dd there was little or no evidence of protein loss (Figure 2A,B), consistent with the lack

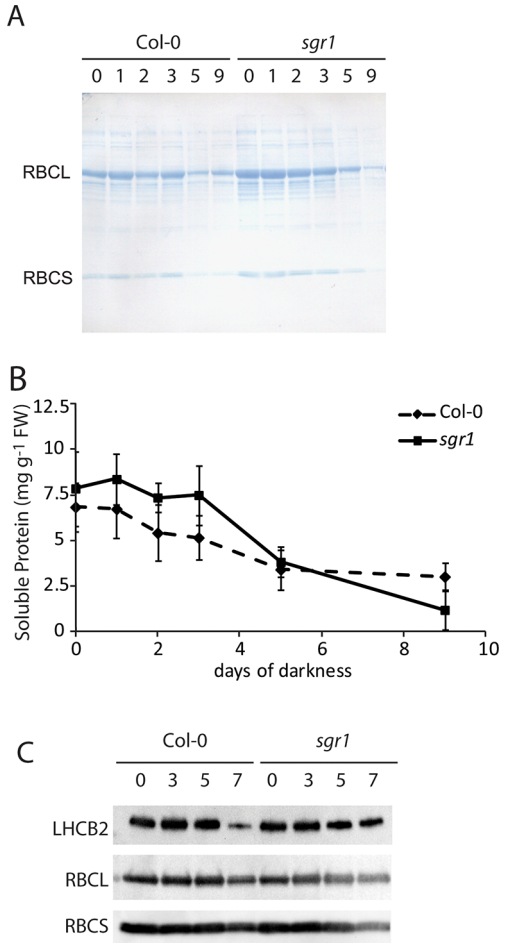

Figure 2. Degradation of proteins in Col-0 and *sgr1* during dark-induced senescence. (A) Soluble proteins from total protein extracts from 0dd, 1dd, 2dd, 3dd, 5dd, and 9dd of Col-0 and *sgr1* leaves separated by SDS-PAGE on FW basis. RBCL, Rubisco large subunit; RBCS, Rubisco small subunit. (B) The soluble protein concentration of leaf extracts on a FW basis of Col-0 and *sgr1* from 0dd, 1dd, 2dd, 3dd, 5dd, and 9dd (mean ± SD, n = 5). (C) Blots were probed with LHCB2 (light harvesting chlorophyll-a/b binding subunit 2), RBCL (Rubisco large subunit) and RBCS (Rubisco small subunit). SDS-PAGE for the membrane protein LHCB2 were loaded on the basis of FW (3.3 mg) and from soluble RBCL and RBCS proteins based on protein (2 ug) using extracts from 0dd, 3dd, 5dd and 7dd Col-0 and *sgr1* leaves.

of Chl breakdown (Figure 1B). Whereas by 5dd, net protein loss associated with senescence had clearly started and the protein content was reduced by 30−40% from the 3dd levels (Figure 2A,B). To determine the timing of the reported stability of LHCB2 in *sgr1*, Western blots were used and showed reduced amounts after 7dd in the WT but more stable levels in *sgr1*. Figure 2B further shows that there is very little difference in protein concentration and amount between Col-0 and *sgr*, at a given time point.

From the results in Figures 1 and 2, it was clear that WT and *sgr1* were similar to each other, in terms of the traits measured at 0dd, and that senescence-induced net protein degradation is not initiated until after 3dd. On the basis of this evidence, 0dd was chosen to study the initial state of both genotypes and 3dd

dx.doi.org/10.1021/pr300691k | J. Proteome Res. 2012, 11, 5443−5452

Table 1. Number of Significant Changes in Plastid Protein Abundance between *sgr1* and Col-0 across Chloroplastic Functional Categories at Different Times during Dark-Induced Senescence[a]

Functional Group	non-reduntant proteins	quant measurements	higher at 0dd	lower at 0dd	higher at 3/5dd	lower at 3d/5dd	non-redund. Sign change:	% non-redund. proteins with sig. change	2-tailed z-stat p-value
Amino acid metabolism	8	15	0	2	2	1	3	38%	0.78^
ATP synthase	4	3	0	1	0	2	2	50%	0.76^
biotic and abiotic stress	14	27	0	3	3	0	5	36%	0.63
Calvin cycle	25	72	8	2	10	12	19	76%	0.0017*
carbohydrate metabolism	6	11	0	0	1	0	1	17%	0.21^
FA synthesis and elongation	3	6	0	1	0	0	1	33%	0.76^
miscellaneous	27	41	2	2	1	2	5	19%	0.019*
nucleotide metabolism	5	6	0	0	1	1	2	40%	0.92^
organic acid metabolism	5	11	3	1	2	1	4	80%	0.1^
protein degradation	9	12	0	0	2	0	2	22%	0.23^
protein synthesis	8	14	1	0	1	0	2	25%	0.33^
PS other	7	15	1	1	1	0	3	43%	0.52
PSI	2	2	0	0	0	0	0	0%	0.23^
PSII	11	27	0	6	3	4	9	82%	0.011*
redox regulation	15	32	0	4	2	0	5	33%	0.50
RNA regulation	4	9	0	2	1	2	3	75%	0.19^
tetrapyrrole synthesis	3	5	0	0	0	0	0	0%	0.15^
total number	**156**	**308**	**15**	**25**	**30**	**25**	**66**	**42%**	

[a]Non-redundant proteins, unique protein list in each category; quant measurements, number of iTRAQ quantified treatment by protein combinations identified across 0dd, 3dd, and 5dd samples; higher at 0dd, number of treatment by protein values higher in *sgr1* at 0dd; lower at 0dd, number of treatment by protein values higher in *sgr1* at 0dd; higher at 3/5dd, number of treatment by protein values higher in *sgr1* at 3 and/or 5dd; lower at 3/5dd, number of treatment by protein values higher in *sgr1* at 3 and/or 5dd; non-redundant. Sign changes, number of unique proteins in each category with significant differences in protein abundance; % non-redundant proteins with sig. change, percentage of total number of unique proteins changing in abundance; 2 tailed z-statl p-value, *p*-value of *z*-test for significant difference from the null hypothesis of random distribution, *, significant at $p < 0.05$; ∧, insufficient sized sets to assess the significance of the *p*-value.

was chosen to study early events during the initiation of senescence. At 5dd, the protein breakdown and remobilization processes appeared to be in progress (Figure 2A,B), Chl contents differed (Figure 1B) and senescence associated gene induction was peaking (Figure 1D). Therefore, 5dd was chosen as a point of advanced senescence which was most different with respect to Chl content in Col-0 and *sgr1*.

Quantitative Comparison of Leaf Plastid Soluble Proteins

Using 0dd, 3dd, and 5dd samples, we then assessed the protein expression changes in the dark-induced leaves of Col-0 and *sgr1*. For iTRAQ-labeling, protein extracts from covered and control leaves from 3 independent plants were prepared and 100 μg of protein was digested with trypsin and labeled with iTRAQ isobaric tags in 3 separate experiments. Using SCX fractionation, 13 peptide-containing fractions were prepared from each replicate and then analyzed by LC−MS/MS. The abundance for each protein was then compared between *sgr1* and Col-0.

At 0dd, 424 proteins were identified and 92 were significantly different in abundance between Col-0 and *sgr1*; at 3dd, 367 proteins were identified and 60 proteins showed significantly different abundance between Col-0 and *sgr1*. At 5dd, 596 proteins were identified and 124 showed significantly different protein abundance. In total, 759 nonredundant proteins were detected across the three time-points. We then filtered our data set to ensure an FDR of <0.05 at the peptide level and by subcellular location by interrogating the SUBA database[14] and found 156 proteins passed this filter and were known from previous experimental evidence to reside in the chloroplast, the site of action of *sgr1*.[6,7,9] In this set of 156 proteins, 66 proteins were statistically significantly different in abundance in the mutant at one time point at least.

Using the Mapman analysis package[15] to classify protein abundance changes into metabolic pathways, we were able to classify many of the proteins identified into a set of 16 chloroplastic functional groups. In total, 76% of the proteins identified in the Calvin cycle and 82% of proteins identified as PSII proteins changed in abundance between Col-0 and *sgr1*. By assessing the proportion of statistically significant protein changes in each category, it was revealed that the number of Calvin cycle and PSII protein abundance changes is significantly higher than would be expected by random ($p < 0.05$) when compared to the number of changes and the relative numbers in each functional category (Table 1).

Among the soluble PSII proteins identified, quantitated, and found to change in abundance, many were part of the oxygen evolving complex (OEC, Table 2). Many of these proteins are present at reduced levels in the *sgr1* mutant even in 0dd, that is, before the dark treatment began. Conversely, several proteins associated with PSII, but which are not part of the OEC, were increased in abundance in *sgr1* compared to WT after 5dd (Table 2).

Several proteins of the Calvin cycle identified showed statistically significant differences in abundance at one time

dx.doi.org/10.1021/pr300691k | *J. Proteome Res.* 2012, 11, 5443−5452

Table 2. Notable Plastid Proteins with Significantly Different Abundances in sgr1 Compared to Col-0 from Photosystem II, Calvin Cycle, Substrate Dehydrogenases (MDH), and Ammonia Assimilation (GOGAT) Subcategories[a]

Category and Abbreviation	Protein Description	AGI	0dd	3dd	5dd
Photosystem II					
PSB27	photosystem II family protein	AT1G03600.1	**-1.22**	1.15	**1.48**
PPL1	PsbP-like protein 1	AT3G55330.1	1.34	-1.08	**1.32**
PsbP	PS II reaction centre PsbP family protein	AT1G77090.1	---	1.13	**1.74**
PSBP-1	PSII subunit P-1	AT1G06680.1	**-1.05**	**-1.17**	
PSBP-2	PSII subunit P-2	AT2G30790.1	**-1.10**		**-1.06**
PSBO-1	PSII oxygen-evolving complex 1	AT5G66570.1	**-1.17**	-1.19	**-1.38**
PSBO-2	PSII subunit O-2	AT3G50820.1	**-1.22**	-1.20	**-1.39**
PSBQ	PSII subunit QA	AT4G21280.1	**-1.07**	1.06	1.08
PSBQ	PSII subunit Q-2	AT4G05180.1	1.12	-1.02	**-1.16**
Calvin Cycle					
RBCL	Ribulose-bisphosphate carboxylase	ATCG00490.1	1.13	**1.30**	-1.14
RCA	Rubisco activase	AT2G39730.1	**1.61**	**-1.19**	**-1.16**
RBCS1A	Ribulose bisphosphate carboxylase small chain 1A	AT1G67090.1	**1.45**	**-1.01**	1.02
RBCS3B	Ribulose bisphosphate carboxylase small chain 3B	AT5G38410.1	**1.41**		**-1.10**
RBCS2B	Ribulose bisphosphate carboxylase small chain 2B	AT5G38420.1		-1.05	
RBCS1B	Ribulose bisphosphate carboxylase small chain 1B	AT5G38430.1	**1.41**	-1.03	**-1.11**
R-5-P-isomerase	Ribose 5-phosphate isomerase, type A protein	AT3G04790.1	-1.09	-1.02	**1.19**
FBA1	Fructose-bisphosphate aldolase 1	AT2G21330.1	**1.10**	-1.10	-1.11
FBA2	Fructose-bisphosphate aldolase 2	AT4G38970.1	**1.13**	**-1.11**	**-1.14**
PGK1	Phosphoglycerate kinase 1	AT3G12780.1	-1.05	**-1.02**	-1.18
PGK	Phosphoglycerate kinase family protein	AT1G56190.1	**1.04**	**-1.10**	-1.15
Transketolase	Transketolase	AT3G60750.1	-1.14	-1.07	**-1.13**
MDH / GAPDH					
MDH	Malate dehydrogenase	AT3G47520.1	**1.29**		1.14
GAPB	Glyceraldehyde-3-phosphate dehydrogenase B	AT1G42970.1	**-1.10**	**1.13**	**1.36**
GAPA-1	Glyceraldehyde 3-phosphate dehydrogenase A	AT3G26650.1	-1.05	**1.22**	**1.43**
GAPA-2	Glyceraldehyde 3-phosphate dehydrogenase A	AT1G12900.1	-1.08	**1.20**	**1.31**
GS/ GOGAT					
GS2	glutamine synthetase 2 (GLN2, ATGSL1)	AT5G35630.1	**-1.04**		**-1.34**
GLU1	glutamate synthase 1 (GLS1, GLUS, FD-GOGAT)	AT5G04140.1	**-1.02**	**-1.06**	

[a]Protein abundance differences between *sgr1* and Col-0 following exposure to 0dd, 3dd, and 5dd. Fold-change differences in abundance for each protein are shown below each independent experiment. Bold and colored numbers show proteins that were statistically significantly greater (green) and lower (red) in abundance ($p > 0.05$, $n = 3$). AGI, Arabidopsis Gene Initiative locus; 0dd, 0 days of darkness; 3dd, 3 days of darkness; 5dd, 5 days of darkness. MDH, malate dehydrogenase; GAPDH, glyceraldehyde-3-phosphate dehydrogenase; GS, glutamine synthetase; GOGAT, glutamine:2-oxoglutarate aminotransferase; PSII, photosystem II. iTRAQ ratios for peptides of PSB Q, P and O at each timepoint are provided in Supplementary Data 3.

point at least in *sgr1* but the direction and amplitude of changes was variable (Table 2). Total protein extracts had shown that *sgr1* contained more protein on a fresh weight basis than WT (Figure 2A,B) in light conditions and this was likely due to higher Rubisco abundance in *sgr1* than WT before dark treatment (0dd). However, after 3dd and 5dd, these two proteins showed less of a difference in abundance between WT and *sgr1*, indicating a reduction in the stability of Rubisco during dark-induced senescence in *sgr1*. While the major Calvin cycle enzyme fructose-bisphosphate aldolase showed a similar pattern of abundance to Rubisco, both isoforms of glyceraldehyde-3-phosphate dehydrogenase (GAPDH) showed an opposite response. GAPDH started at similar abundance in both the WT and *sgr1* at 0dd and rose to a greater relative abundance in *sgr1* than WT over time in the dark (Table 2).

Besides PSII and the Calvin cycle, a number of other prominent abundance changes were also evident in the chloroplast protein set (Table 1). The apparently lower abundance in *sgr1* of thioredoxins and peroxiredoxins (Supplementary Data S1), known to reduce protein disulfides and detoxify ROS, and higher abundance of substrate dehydrogenases that drive reduction of the NAD^+ pool, such

dx.doi.org/10.1021/pr300691k | J. Proteome Res. 2012, 11, 5443−5452

as GAPDH and MDH (Table 2), could suggest a more reducing environment is maintained during dark-induced senescence in the mutant. In SGR-overexpression lines, enhanced disassembly of LHCs of PSII produces singlet oxygen[16] possibly explaining why altered reducing conditions could be associated with altered SGR abundance. Nitrogen remobilisation during senescence largely stems from protein breakdown to amino acids and three major protein degradation pathways have been recognized to be involved in this process: the ubiquitin proteasome system, chloroplast degradation and vacuolar and autophagic degradation.[17−19] Chloroplast proteins account for more than 70% of total leaf protein and their proteolysis provides a large pool of cellular nitrogen for recycling during senescence.[10] As both GS and GOGAT were lower in abundance in *sgr1* (Table 2) during the dark treatment, this could result in differential proteolysis or N recycling in *sgr1*. This could be linked to differences in yields reported for *sgr1* crop plants due to differing kinetics of N retrieval from senescing leaf material.[2,10] Clp proteases are known to be involved in protein degradation during leaf senescence in *Arabidopsis*.[20,21] However, although a number of Clp subunits were identified, no consistent significant differences could be observed before or during the darkness treatment in the *sgr1* mutant (Supplementary Data S1). Proteins involved in the chlorophyll synthesis or degradation pathways known to be associated with LHCII were not identified in this proteome screen, suggesting that they are of low abundance or tightly associated with the membrane.[9]

Loss of Oxygen Evolving Complex Subunits in *sgr1*

The quantitative proteomic analysis of soluble protein fractions showed that PsbQ, PsbP, and PsbO, the main constituents of the OEC, are reduced in abundance in *sgr1* compared to the WT, both prior to and throughout the dark treatment (Table 2, Supplementary Data 3). To verify these observations and deduce if these differences reflected actual loss of OEC components on a whole leaf basis, we performed Western blotting on both soluble and membrane extracts using PsbQ, PsbP, and PsbO antibodies (Figure 3). Western blotting of both the soluble and the membrane fractions showed that after 3dd and further at 5dd the amount of PsbQ, PsbP, and PsbO decreased in *sgr1* compared to the WT in both soluble (i.e., iTRAQ assessed fractions), and in membrane fraction where the bulk of the OEC is expected to reside. The results showed that PsbO is mostly located in the membrane fraction while PsbP and PsbQ are present in equal amounts in the soluble and membrane fractions. Overall, it appears that the total OEC protein content was decreased in abundance in both WT and *sgr1* during the dark treatment. The difference between *sgr1* and WT after 5dd was more pronounced in the membrane fraction. Interestingly, the iTRAQ analysis uncovered that PPL proteins (Psb27, PPL, PsbP-like) were relatively more abundant in *sgr1* after 5dd. These proteins are known to be involved in the repair of the OEC.[22,23] Their relative higher abundance may be a response of the plant to the loss of the OEC proteins and/or the lack of disassembly of the LHCs in PSII.

Lower Photosynthetic Capacity in *sgr1* after Prolonged Darkness

The observation of the altered Calvin cycle, PSII LHC, and PSII OEC components in the mutant is likely to have significant effects on photosynthetic gas exchange properties of *sgr1*. To examine this, we performed analysis of CO_2 assimilation rate, stomatal conductance, and internal CO_2 concentration in both WT and *sgr1* plants recovered from darkness at different times.

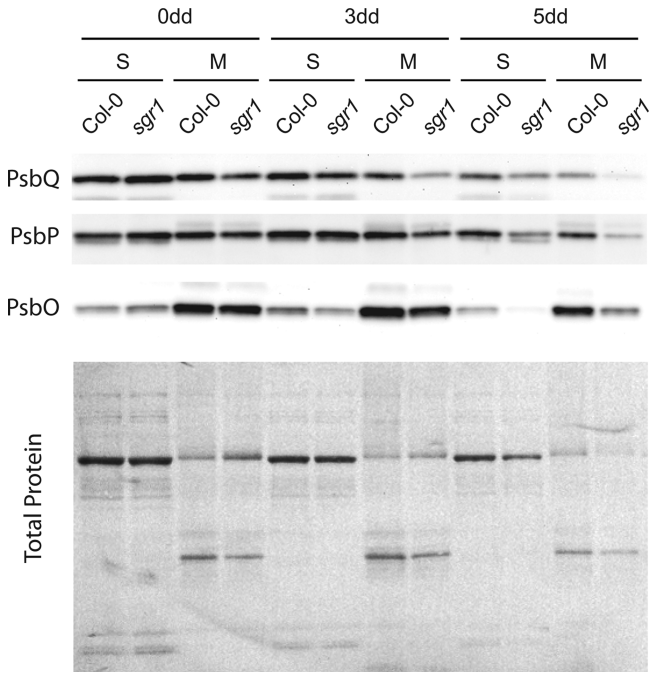

Figure 3. Oxygen evolving complex composition during dark-induced senescence. Western blots of soluble and membrane proteins from 0dd, 3dd, and 5dd of Col-0 and *sgr1* leaves separated by SDS-PAGE on FW basis. Blots were performed with antibodies against PSII oxygen evolving complex proteins: PsbQ (Photosystem II subunit Q), PsbP (Photosystem II subunit P), and PsbO (Photosystem II subunit O). Changes in soluble and membrane protein on a FW basis are indicated in the naphtal protein stain.

The photosynthetic rate of *sgr1* mutant was not significantly lower than in WT before the dark treatment. CO_2 assimilation versus internal CO_2 concentration (A/Ci) curves at 0dd did not reveal any significant difference in the kinetics of assimilation rate (Figure 4A). However, after 3dd, assimilation rates became significantly different between WT and the mutant, which is consistent with the differential decrease in OEC proteins in *sgr1* (Figure 4B). The stomatal conductance and calculated internal CO_2 concentration were slightly increased following periods of dark-induced senescence but were not significantly different between WT and *sgr1* (Figure 4C,D). Together these results show that the reduction of photosynthetic gas exchange in *sgr1* is most likely to be due to reductions on OEC proteins and not to limitations in leaf CO_2 supply or assimilation rate.

DISCUSSION

Evidence for Differences in *sgr1* before the Onset of Senescence

A quantitative proteomic analysis of the type C stay-green mutant *sgr1* revealed that 15 proteins located in the plastid were more abundant and 25 were less abundant than WT in normal growth conditions (0dd) (Table 1). Interestingly, the most highly induced and highly repressed proteins have unknown function in *Arabidopsis*. The most induced protein at 0dd is member of the plastid-lipid associated protein (PAP) family (At2g35490) which is known to coexpress with Var2, ClpR isforms and a range of thioredoxins.[24] The most depleted protein in *sgr1* before the onset of senescence was an acyl

dx.doi.org/10.1021/pr300691k | J. Proteome Res. 2012, 11, 5443−5452

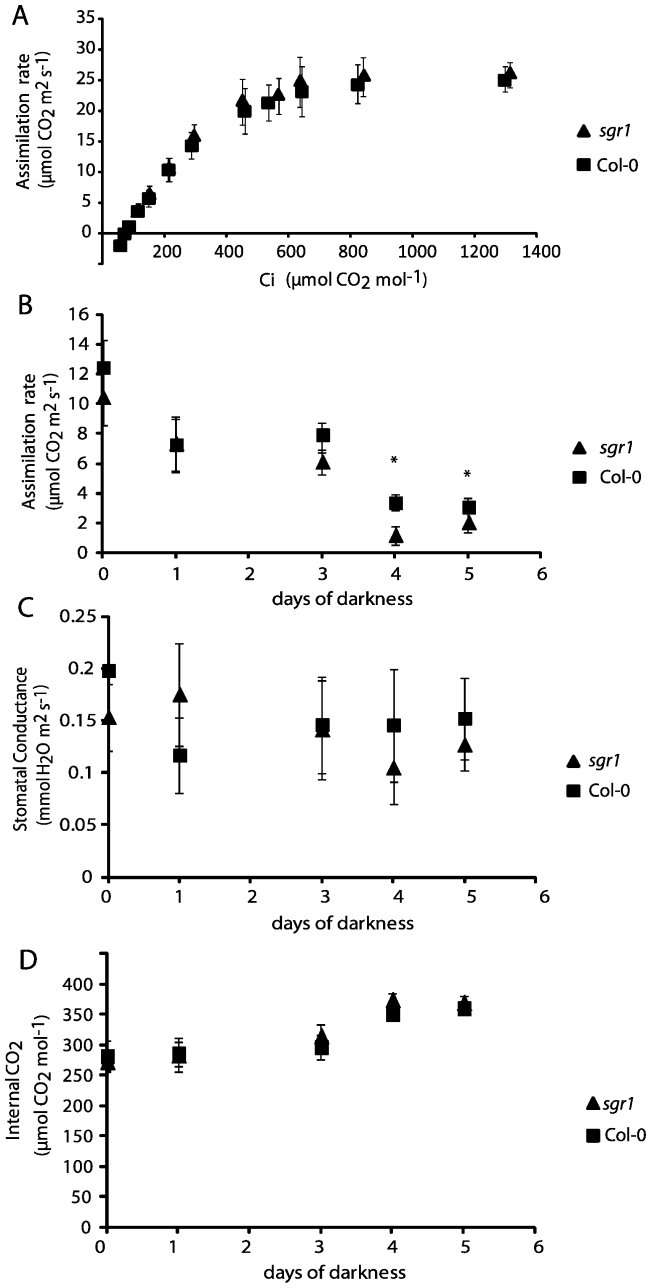

Figure 4. Photosynthetic activity, stomatal conductance and internal CO_2 concentration of leaves recovered after different times of dark-induced senescence. (A) Photosynthetic assimilation rate at different CO_2 concentrations (A/Ci curve) of *sgr1* and Col-0 at 0dd. (B) Photosynthetic assimilation rate of *sgr1* and Col-0 after 0, 1, 3, 4, and 5 days of darkness. (C) Stomatal conductance of *sgr1* and Col-0 after 0, 1, 3, 4, and 5 days of darkness. (D) Internal CO_2 concentration. Measured after equilibration to similar conditions as plants were grown (see Material and Methods). Error bars show the standard deviation, and asterisk (*) indicates statistically significant difference ($p < 0.05$, $n = 5$) from Col-0.

carrier protein 4 (At4g25050) which is coexpressed with plastid ribosome subunits and transcriptionally responsive to light.[24,25] This protein has been repeatedly identified in plastid proteome studies as a stromal-located protein,[26−28] but its exact function has not been studied to date.

The most dramatic differences in protein abundance at 0dd were the increased abundance of Rubisco and Rubisco activase, aldolase and carbonic anhydrase, pointing to an enhanced maximum capacity for CO_2 assimilation. Adjustment of this most basic of plastid processes even before dark treatment shows that the effect of SGR1 deficiency is not exclusively related to chlorophyll breakdown during senescence, but that SGR may act upstream of the senescence program in the cell. During the Calvin cycle, CO_2 assimilation by Rubisco is the rate-limiting step. The quantitative proteomic analysis showed that the Calvin cycle was already modified before darkness treatment in *sgr1* compared to the WT. This indicates that photosynthesis could be modified in the mutant even before the onset of senescence, generating a new metabolic state within the chloroplast. The subsequent changes in the Calvin cycle during darkness might thus originate from this pre-existing alteration in plastid composition. Other major differences in *sgr1* included a lower abundance of proteins involved in redox homeostasis and antioxidant defense (GR, SAPX, PRXQ, 2-Cys Prx B, Thioredoxin M). This is notable, because during senescence these redox and antioxidant proteins were seen to increase in abundance in the WT relative to *sgr1*. Similarly, OCR components of PSII (PSPQ, PSPB) were seen to be lower in abundance in *sgr1* when compared to WT even at 0dd.

Alterations of Plastid Metabolism in *sgr1* during Early Senescence

It is known that leaf senescence is accompanied by the degradation of proteins, lipids, and nucleic acids, and extensive gene expression changes are associated with these processes.[29] To date, the precise mechanism of SGR function remains unknown.[4,30] It was generally thought that SGR works specifically in green plastids and this view has been formed by many reports that focus on its role in these organelles. However, this exclusive localization has recently been questioned by recent evidence that SGR is both expressed in roots and its loss can affect root nodule development and nodule senescence in alfalfa.[30] In our quantitative proteomics analysis, nearly 40% of the proteins with altered expression in *sgr1*/WT comparisons were located in the chloroplast; however, no obvious changes in abundance were observed in proteins directly involved in either Chl synthesis or degradation.

The most striking differences seen during dark induced senescence in *sgr1* were the greater abundance of GAPDH, and an enzyme involved in the biosynthesis of cysteine (OASB). This combination is likely to lead to a more reducing environment in *sgr1* during the darkened period. This would help prevent chlorophyll oxidation and other oxidative events that might otherwise promote senescence processes.[31,32] Dark-induced oxidative damage leading to enhanced senescence has been observed in wheat, where the dark-induced loss of antioxidant defenses has been pinpointed as the cause of H_2O_2 accumulation.[33] Blue light was shown to reduce this effect and prevent loss of catalase activity during dark-induced senescence in wheat.[34]

A second area of major difference between *sgr1* and WT is the ammonia assimilation machinery. Levels of GS and GOGAT were significantly lower in *sgr1* than WT. In senescing leaves, nitrogen net flux is focused toward remobilisation from nitrogen reserves, such as proteins, to small nitrogenous metabolites such as amino acids, that can be exported from the senescing leaf.[35] Estimates suggest that three-quarters of the nitrogen present in mesophyll is in the chloroplasts, with

dx.doi.org/10.1021/pr300691k | J. Proteome Res. 2012, 11, 5443−5452

Rubisco representing the major fraction.[36] The rate of senescence and the remobilization of leaf nitrogen are related to the nitrogen nutrition status of the plant and on source/sink relations with surrounding tissues. In this context assimilation of ammonia as a consequence of deamination events is likely to be an important component in the orderly progression of senescence. A range of reports have noted induction of ammonia assimilation enzymes in specific regions of leaves during senescence.[37,38] Reduced levels of components of ammonia assimilation could hamper this process in *sgr1* with progressing darkness.

A Differential Role of SGR in Stabilization of Different Modules of PSII

Chlorophyll exists in chlorophyll−protein complexes in plastids, where it plays a central role in light energy absorption during photosynthesis. Higher plants contain a number of Chl−protein complexes, most notably PSI and PSII reaction center complexes and the cytochrome b_6f complex, that contain varying amounts of two Chl forms, Chl *a* and Chl *b*. The onset of Chl degradation is an important step for degradation of Chl−protein complexes themselves, especially in the case of LHCII. Evidence has been reported in several species that greenness of *SGR* mutants plants is mainly associated with a failure in the disassembling mechanism of intact LHCP complexes in the thylakoid membranes, which is a prerequisite for the degradation of Chls and Chl-free LHCPs during senescence.[7,9] Our results are consistent with this, in that LHCs remain intact in the *sgr* mutant alongside the retention of Chl. However, OEC, the module of PSII that oxidizes water to oxygen, is more rapidly degraded in *sgr1* than WT. The decrease of OEC in combination with LHCII retention likely leads to a higher oxidized state of Chl in *sgr1* than in WT in the dark. Both PPL and PSB27 were more abundant in *sgr1* as senescence progressed. Both these proteins are noncatalytic oxygen-evolving complex proteins, associated with repair of PSII from oxidative damage.[22,23] Thus, the possibly increased oxidative damage may be counteracted by the observed increase of proteins for antioxidative control of PSII.

CONCLUSION

Our quantitative proteomics approach has revealed 66 plastid proteins that were either down- or up-regulated in the *sgr1* mutant before or during senescence, a number unknown among functioning plastid proteins. On the basis of the analysis of this data set, we observed that SGR directly or indirectly affects the expression or the rate of degradation of a large number of plastid proteins involved in different metabolic and biosynthetic processes. The global protein profiling analysis of the *sgr1* mutant thus provides valuable data for further research in elucidating functional mechanisms of SGR and points to a new hypothesis of a role for SGR in modulating the stability of the OEC of PSII, the redox homeostasis of the stroma, and potentially the redox status of LHCs in defining the rate of dark-induced Chl degradation.

ASSOCIATED CONTENT

Supporting Information

Supplementary Data S1, plastid proteins significantly changed in abundance in *sgr1* compared to Col-0 following 0, 3, and 5 days of darkness; Supplementary Data 2, peptide MS/MS spectra for protein identification at different time points based in single peptides with ion score >34/35 (FDR 5%); Supplementary Data 3, ITRAQ data sets for PSB-P, PSB-Q, PSB-O proteins showing ratios of individual peptides used in the statistical calculation of protein ratios. This material is available free of charge via the Internet at http://pubs.acs.org.

AUTHOR INFORMATION

Corresponding Author

*Address: ARC Centre of Excellence in Plant Energy Biology and Centre for Comparative Analysis of Biomolecular Networks, The University of Western Australia (M316), 35 Stirling Highway, Crawley 6009 WA, Australia. Tel: +61 8 6488 7245. Fax: +61 8 64884401. E-mail: harvey.millar@uwa.edu.au.

Notes

The authors declare no competing financial interest.

ACKNOWLEDGMENTS

This work was supported by the Australian Research Council (ARC) through an Australian Future Fellowship to A.H.M. (FT110100242) and an ARC Discovery Grant to A.H.M. and N.L.T. (DP0985873).

REFERENCES

(1) Hörtensteiner, S. Chlorophyll degradation during senescence. *Ann. Rev. Plant Biol.* **2006**, *57*, 55−77.
(2) Yoo, S. C.; Cho, S. H.; Zhang, H.; Paik, H. C.; Lee, C. H.; Li, J.; Yoo, J. H.; Lee, B. W.; Koh, H. J.; Seo, H. S.; Paek, N. C. Quantitative trait loci associated with functional stay-green SNU-SG1 in rice. *Mol. Cells* **2007**, *24*, 83−94.
(3) Thomas, H.; Howarth, C. J. Five ways to stay green. *J. Exp. Bot.* **2000**, *51*, 329−337.
(4) Hörtensteiner, S. Stay-green regulates chlorophyll and chlorophyll-binding protein degradation during senescence. *Trends Plant Sci.* **2009**, *14*, 155−162.
(5) Armstead, I.; Donnison, I.; Aubry, S.; Harper, J.; Hörtensteiner, S.; James, C.; Mani, J.; Moffet, M.; Ougham, H.; Roberts, L.; Thomas, A.; Weeden, N.; Thomas, H.; King, I. Cross-species identification of Mendel's I locus. *Science* **2007**, *315*, 73.
(6) Ren, G.; An, K.; Liao, Y.; Zhou, X.; Cao, Y.; Zhao, H.; Ge, X.; Kuai, B. Identification of a novel chloroplast protein AtNYE1 regulating chlorophyll degradation during leaf senescence in Arabidopsis. *Plant Physiol.* **2007**, *144*, 1429−1441.
(7) Park, S. Y.; Yu, J. W.; Park, J. S.; Li, J.; Yoo, S. C.; Lee, N. Y.; Lee, S. K.; Jeong, S. W.; Seo, H. S.; Koh, H. J.; Jeon, J. S.; Park, Y. I.; Paek, N. C. The senescence-induced staygreen protein regulates chlorophyll degradation. *Plant Cell* **2007**, *19*, 1649−1664.
(8) Sato, Y.; Morita, R.; Nishimura, M.; Yamaguchi, H.; Kusaba, M. Mendel's green cotyledon gene encodes a positive regulator of the chlorophyll-degrading pathway. *Proc. Natl Acad. Sci. U.S.A.* **2007**, *104*, 14169−14174.
(9) Sakuraba, Y.; Schelbert, S.; Park, S. Y.; Han, S. H.; Lee, B. D.; Andres, C. B.; Kessler, F.; Hörtensteiner, S.; Paek, N. C. STAY-GREEN and chlorophyll catabolic enzymes interact at light-harvesting complex II for chlorophyll detoxification during leaf senescence in Arabidopsis. *Plant Cell* **2012**, *24*, 507−518.
(10) Thomas, H.; Ougham, H.; Canter, P.; Donnison, I. What stay-green mutants tell us about nitrogen remobilization in leaf senescence. *J .Exp. Bot* . **2002**, *53*, 801−808.
(11) Mecey, C.; Hauck, P.; Trapp, M.; Pumplin, N.; Plovanich, A.; Yao, J.; He, S. Y. A critical role of STAYGREEN/Mendel's I locus in controlling disease symptom development during Pseudomonas syringae pv tomato infection of Arabidopsis. *Plant Physiol.* **2011**, *157*, 1965−1974.
(12) Mur, L. A.; Aubry, S.; Mondhe, M.; Kingston-Smith, A.; Gallagher, J.; Timms-Taravella, E.; James, C.; Papp, I.; Hörtensteiner, S.; Thomas, H.; Ougham, H. Accumulation of chlorophyll catabolites

photosensitizes the hypersensitive response elicited by *Pseudomonas syringae* in Arabidopsis. *New Phytol.* **2010**, *188*, 161−174.
(13) Aubry, S.; Mani, J.; Hörtensteiner, S. Stay-green protein, defective in Mendel's green cotyledon mutant, acts independent and upstream of pheophorbide a oxygenase in the chlorophyll catabolic pathway. *Plant Mol. Biol.* **2008**, *67*, 243−256.
(14) Heazlewood, J. L.; Verboom, R. E.; Tonti-Filippini, J.; Small, I.; Millar, A. H. SUBA: the Arabidopsis Subcellular Database. *Nucleic Acids Res.* **2007**, *35*, D213−D218.
(15) Thimm, O.; Blaesing, O.; Gibon, Y.; Nagel, A.; Meyer, S.; Krüger, P.; Selbig, J.; Müller, L. A.; Rhee, S. Y.; Stitt, M. MAPMAN: a user-driven tool to display genomics data sets onto diagrams of metabolic pathways and other biological processes. *Plant J.* **2004**, *37*, 914−939.
(16) Jiang, H.; Chen, Y.; Li, M.; Xu, X.; Wu, G. Overexpression of SGR results in oxidative stress and lesion-mimic cell death in rice seedlings. *J. Integr. Plant Biol.* **2011**, *53*, 375−387.
(17) Buchanan-Wollaston, V. The molecular biology of leaf senescence. *J. Exp. Bot.* **1997**, *48*, 181−199.
(18) Martinez, D. E.; Costa, M. L.; Gomez, F. M.; Otegui, M. S.; Guiamet, J. J. Senescence-associated vacuoles' are involved in the degradation of chloroplast proteins in tobacco leaves. *Plant J.* **2008**, *56*, 196−206.
(19) Balazadeh, S.; Parlitz, S.; Mueller-Roeber, B.; Meyer, R. C. Natural developmental variations in leaf and plant senescence in Arabidopsis thaliana. *Plant Biol.* **2008**, *10*, 136−147.
(20) Nakabayashi, K.; Ito, M.; Kiyosue, T.; Shinozaki, K.; Watanabe, A. Identification of clp genes expressed in senescing Arabidopsis leaves. *Plant Cell Physiol.* **1999**, *40*, 504−514.
(21) Nakashima, K.; Kiyosue, T.; Yamaguchi-Shinozaki, K.; Shinozaki, K. A nuclear gene, erd1, encoding a chloroplast-targeted Clp protease regulatory subunit homolog is not only induced by water stress but also developmentally up-regulated during senescence in *Arabidopsis thaliana*. *Plant J.* **1997**, *12*, 851−861.
(22) Chen, H.; Zhang, D.; Guo, J.; Wu, H.; Jin, M.; Lu, Q.; Lu, C.; Zhang, L.; Psb2, A homologue in Arabidopsis thaliana is required for efficient repair of photodamaged photosystem II. *Plant Mol. Biol.* **2006**, *61*, 567−575.
(23) Ishihara, S.; Takabayashi, A.; Ido, K.; Endo, T.; Ifuku, K.; Sato, F. Distinct functions for the two PsbP-like proteins PPL1 and PPL2 in the chloroplast thylakoid lumen of Arabidopsis. *Plant Physiol.* **2007**, *145*, 668−679.
(24) Toufighi, K.; Brady, S. M.; Austin, R.; Ly, E.; Provart, N. J. The Botany Array Resource: e-Northerns, expression angling, and promoter analyses. *Plant J.* **2005**, *43*, 153−163.
(25) Bonaventure, G.; Ohlrogge, J. B. Differential regulation of mRNA levels of acyl carrier protein isoforms in Arabidopsis. *Plant Physiol.* **2002**, *128*, 223−235.
(26) Ferro, M.; Brugiere, S.; Salvi, D.; Seigneurin-Berny, D.; Court, M.; Moyet, L.; Ramus, C.; Miras, S.; Mellal, M.; Le Gall, S.; Kieffer-Jaquinod, S.; Bruley, C.; Garin, J.; Joyard, J.; Masselon, C.; Rolland, N. AT-CHLORO, a comprehensive chloroplast proteome database with subplastidial localization and curated information on envelope proteins. *Mol. Cell. Proteomics* **2010**, *9*, 1063−1084.
(27) Olinares, P. D.; Ponnala, L.; van Wijk, K. J. Megadalton complexes in the chloroplast stroma of *Arabidopsis thaliana* characterized by size exclusion chromatography, mass spectrometry, and hierarchical clustering. *Mol. Cell. Proteomics* **2010**, *9*, 1594−1615.
(28) Zybailov, B.; Rutschow, H.; Friso, G.; Rudella, A.; Emanuelsson, O.; Sun, Q.; van Wijk, K. J. Sorting signals, N-terminal modifications and abundance of the chloroplast proteome. *PLoS One* **2008**, *3*, e1994.
(29) Buchanan-Wollaston, V.; Earl, S.; Harrison, E.; Mathas, E.; Navabpour, S.; Page, T.; Pink, D. The molecular analysis of leaf senescence-a genomics approach. *Plant Biotechnol. J.* **2003**, *1*, 3−22.
(30) Zhou, C.; Han, L.; Pislariu, C.; Nakashima, J.; Fu, C.; Jiang, Q.; Quan, L.; Blancaflor, E. B.; Tang, Y.; Bouton, J. H.; Udvardi, M.; Xia, G.; Wang, Z.-Y. From model to crop: functional analysis of a STAY-GREEN gene in the model legume Medicago truncatula and effective use of the gene for alfalfa improvement. *Plant Physiol.* **2011**, *157*, 1483−1496.
(31) Zimmermann, P.; Zentgraf, U. The correlation between oxidative stress and leaf senescence during plant development. *Cell Mol. Biol. Lett.* **2005**, *10*, 515−534.
(32) Zimmermann, P.; Heinlein, C.; Orendi, G.; Zentgraf, U. Senescence-specific regulation of catalases in Arabidopsis thaliana (L.) Heynh. *Plant Cell Environ.* **2006**, *29*, 1049−1060.
(33) Causin, H. F.; Jauregui, R. N.; A.J., B. The effect of light spectral quality on leaf senescence and oxidative stress in wheat. *Plant Sci.* **2006**, *171*, 24−33.
(34) Causin, H. F.; Roberts, I. N.; Criado, M. V.; Gallego, S. M.; Pena, L. B.; del Carmen Ríos, M.; Barneix, A. J. Changes in hydrogen peroxide homeostasis and cytokinin levels contribute to the regulation of shade-induced senescence in wheat leaves. *Plant Sci.* **2009**, *177*, 698−704.
(35) Hörtensteiner, S.; Feller, U. Nitrogen metabolism and remobilization during senescence. *J. Exp. Bot.* **2002**, *53*, 927−937.
(36) Peoples, M. B.; Dalling, M. J. The interplay between proteolysis and amino acid metabolism during senescence and nitrogen reallocation. In *Senescence and Aging in Plants*; Noodén, L. D., Leopold, A. C., Eds.; Academic Press: San Diego, CA, 1988; pp 181−217.
(37) Kichey, T.; Le Gouis, J.; Sangwan, B.; Hirel, B.; Dubois, F. Changes in the cellular and subcellular localization of glutamine synthetase and glutamate dehydrogenase during flag leaf senescence in wheat (*Triticum aestivum* L.). *Plant Cell Physiol.* **2005**, *46*, 964−974.
(38) Brugière, N.; Dubois, F.; Masclaux, C.; Sangwan, R. S.; Hirel, B. Immunolocalization of glutamine synthetase in senescing tobacco (Nicotiana tabacum L.) leaves suggests that ammonia assimilation is progressively shifted to the mesophyll cytosol. *Planta* **2000**, *211*, 519−527.